Developmental Biology 463 (2020) 26–38

Contents lists available at ScienceDirect

Developmental Biology

journal homepage: www.elsevier.com/locate/developmentalbiology

Desert hedgehog-primary cilia cross talk shapes mitral valve tissue by organizing smooth muscle actin

Diana Fulmer [a], Katelynn A. Toomer [a,c], Janiece Glover [a], Lilong Guo [a], Kelsey Moore [a], Reece Moore [a], Rebecca Stairley [a], Cortney Gensemer [a], Sameer Abrol [a], Mary Kate Rumph [a], Faith Emetu [a], Joshua H. Lipschutz [b], Colin McDowell [a], Justin Bian [a], Christina Wang [a], Tyler Beck [a], Andy Wessels [a], Marie-Ange Renault [d], Russell A. Norris [a,b,*]

[a] Department of Regenerative Medicine and Cell Biology, Medical University of South Carolina, Charleston, SC, USA
[b] Department of Medicine, Medical University of South Carolina, Charleston, SC, USA
[c] Department of Genetic Medicine, John Hopkins, Baltimore, MD, USA
[d] Inserm U1034, University of Bordeaux, Pessac, France

ARTICLE INFO

Keywords:
Primary cilia
Desert hedgehog signaling
Valve development
Myxomatous degeneration

ABSTRACT

Non-syndromic mitral valve prolapse (MVP) is the most common heart valve disease affecting 2.4% of the population. Recent studies have identified genetic defects in primary cilia as causative to MVP, although the mechanism of their action is currently unknown. Using a series of gene inactivation approaches, we define a paracrine mechanism by which endocardially-expressed Desert Hedgehog (DHH) activates primary cilia signaling on neighboring valve interstitial cells. High-resolution imaging and functional assays show that DHH de-represses smoothened at the primary cilia, resulting in kinase activation of RAC1 through the RAC1-GEF, TIAM1. Activation of this non-canonical hedgehog pathway stimulates α-smooth actin organization and ECM remodeling. Genetic or pharmacological perturbation of this pathway results in enlarged valves that progress to a myxomatous phenotype, similar to valves seen in MVP patients. These data identify a potential molecular origin for MVP as well as establish a paracrine DHH-primary cilium cross-talk mechanism that is likely applicable across developmental tissue types.

1. Introduction

Mitral valve prolapse (MVP) is a progressive cardiac tissue disorder that affects 1 in 40 individuals worldwide (Levine et al., 1989, 2018; Delling et al., 2014, 2016; Freed et al., 1999, 2002). It is characterized by destruction of the extracellular matrix (ECM), which disrupts the valvular tissue architecture and renders the valves biomechanically incompetent. Patients with MVP often develop secondary complications including arrhythmias, heart failure and sudden cardiac death unless surgically corrected (Basso et al., 2015; Devereux et al., 1989; Perloff and Child, 1987). Recent work has linked MVP to inborn errors of valve development and has identified variants in genes that are important for the formation and function of primary cilia (Yu et al., 2019; Toomer et al., 2019a; Durst et al., 2015). Primary cilia are singular, immotile projections of microtubules that extend from the surface of cells into the extracellular space. Although originally considered evolutionary remnants, primary cilia are now known to function as mechanosensors and signaling hubs to regulate many developmental processes. These structures possess complex repertoires of channel proteins and membrane-associated receptors that transduce chemical, electrical and mechanical cues from the surrounding microenvironment to control various cellular responses (Gerhardt et al., 2016; Nauli et al., 2013; Goto et al., 2013; Broekhuis et al., 2013; Seeger-Nukpezah and Golemis, 2012; Lienkamp et al., 2012; Hsiao et al., 2012; Davis and Katsanis, 2012; Ishikawa and Marshall, 2011; Hildebrandt et al., 2011; Veland et al., 2009; Gerdes and Katsanis, 2008; Christensen et al., 2008; Delling et al., 2013).

The hedgehog pathway is a well-established growth factor signaling pathway that requires the primary cilium for its function (Seeger-Nukpezah and Golemis, 2012; Hildebrandt et al., 2011; Veland et al., 2009; Guerrero and Kornberg, 2014; Vokes and McMahon, 2004;

* Corresponding author. Medical University of South Carolina, Department of Regenerative Medicine and Cell Biology, 173 Ashley Ave, BSB 601, Charleston, SC, 29425, USA.
E-mail address: norrisra@musc.edu (R.A. Norris).

https://doi.org/10.1016/j.ydbio.2020.03.003
Received 27 December 2019; Received in revised form 27 February 2020; Accepted 2 March 2020
Available online 6 March 2020

Aza-Blanc and Ci, 1999). The initial input for this signaling cascade is at least one of three hedgehog ligands, Sonic Hedgehog (SHH), Indian Hedgehog (IHH), and/or Desert Hedgehog (DHH). These ligands interact with their cognate receptor, Patched (PTC) along the ciliary axoneme, which results in de-repression of the G-coupled protein receptor, Smoothened (SMO) at the cilia base. The canonical signaling pathway culminates with nuclear translocation of GLI transcriptional activators and/or repressors to modify expression of target genes primarily involved in cell cycle regulation. Due to the broad expression domains of hedgehog ligands and the presence of primary cilia on nearly every cell-type during development, it is not surprising that defects in ciliogenesis and its downstream signaling can cause a wide variety of congenital defects in humans (Davis and Katsanis, 2012; Hildebrandt et al., 2011; Veland et al., 2009; Jin et al., 2017; Karp et al., 2012).

In the heart, primary cilia are observed in the majority of cell types and have been associated with various congenital cardiac defects (Toomer et al., 2017, 2019a; Gerhardt et al., 2016; Jin et al., 2017; Karp et al., 2012; Fulmer et al., 2019; Burns et al., 2019; Li et al., 2015; Samsa et al., 2015; Willaredt et al., 2012; Friedland-Little et al., 2011). Recent genetic and molecular studies have established primary cilia as important in forming both the mitral and aortic valves (Toomer et al., 2017, 2019a; Fulmer et al., 2019). However, how primary cilia function and whether hedgehog ligands are involved in cilia signaling during valve morphogenesis is currently unknown. Through a combination of *in vivo* and *in vitro* analyses, we show that among the three hedgehog ligands, only Desert Hedgehog (DHH) functions during fetal gestation to regulate cytoskeletal organization of the valve leaflets through a non-canonical, cilia-dependent pathway. The hedgehog signal emanates from the endocardium and is received by ciliated valve interstitial cells (VICs). This paracrine cross-talk is specific to developmental time points and is critical for shaping the valve into a thin, attenuated structure. Genetic perturbation of this pathway results in valvular defects during fetal gestation and leads to the generation of myxomatous valves later in life. Our studies establish a molecular and developmental origin for myxomatous mitral valves through a novel cross-talk mechanism and further implicate MVP as a congenital defect.

2. Materials and methods

The data that support the findings of this study are available from the corresponding author upon reasonable request.

RT-PCR: Reverse transcribed RNA isolated from immortalized mouse mitral valve interstital cells (mVICs) was used for RT-PCR analyses of *Gli1, Gli2, Gli3, Smoothened, Patched 1, Patched 2, Shh, Ihh, Dhh* and *Hprt* (Quantabio, Inc). The mVICs were a kind gift of Dr. Joey Barnett (Vanderbilt University) and previously published (Toomer et al., 2019a; Peng et al., 2016). Primer sequences used: Patched 1: Forward: 5′-TAATGCTG CGACAACTCAGG-3′, Reverse: 5′-GGCTGGAGTCTGAGAACTGG-3′, Patched 2: Forward: 5′-CTTGACTGCTTCTGGGAAGG-3’; Reverse: 5-‘GCCAGCATAAGCAGATAGCC-3’, Smoothened: Forward: 5′-CTGGG AGTCGGTTTTAATGG-3’; Reverse: 5′-ACACGTTGTAGCGCAAAGG-3′, Gli1: Forward: 5′-CGGAGTTCAGTCAAATTAAC-3’; Reverse: 5′-CA TCTGAGGTTGGGAATCC-3′, Gli2: Forward: 5′-AGCCTTCACC-CACCTTCTTG-3’; Reverse: 5′-TGGGCGCAGGCCCTCAGC-3′, Gli3: Forward: 5′-CCTTCTGAGTCCTCACAGAG-3’; Reverse: 5′-GACTAGGGT TGTTCCTTCCG-3′, HPRT: Forward: 5′-GCGATGATGAACCAGGTTA-3’; Reverse: 5′-GTTGAGAGATCATCTCCACC-3′, Shh: Forward: 5′-CAAAAA GCTGACCCCTTTAGC-3’; Reverse: 5′-CGTCTCGATCACGTAGAAGA CC-3′, Ihh: Forward: 5′-CTTGCCTACAAGCAGTTCAGC-3’; Reverse: 5′-TGCTGGTTCTGTATGATTGTCC-3′, Dhh: Forward: 5′-CTTCAAGGAT-GAGGAGAACAGC-3’; Reverse: 5′-TGACTCTCTAGAACCGCGTAGC-3’.

RNAseq. Mitral leaflets were dissected from P0 wildtype mice (n = 3) and RNA was isolated using MicroRNeasy (Qiagen). Purity and quantification was determined by Bioanalyzer and the library preparation was done using the SMART-Seq v4 RNA-seq kit (Clontech Laboratories) per manufacturer instructions. The analysis was conducted on an OnRamp Bioinformatics Genomics research platform as previously described (Toomer et al., 2019a).

In situ hybridizations. In situ hybridizations were performed as previously described (Durst et al., 2015; Norris et al., 2004) and amplified with primers containing a SP6 RNA polymerase site engineered onto the 3′ end of the reverse primer (5′-CGATCATTTAGGTGACACTATA GAAGAACCCCACTCACAGTTGGTATG-3′, SP6 site underlined) or a T7 RNA polymerase site engineered onto the 3′ end (Forward 5′-CGATCTAATACGACTCACTATAGGGAAGGACAGAAGTCCTCCAAG-C-3′, T7 site underlined.) n = 3/timepoint.

Mouse husbandry and genotyping. Animals were kept in a 12-h light-dark cycle with food and water *ad libitum*. Genotyping was performed by Transnetyx, Inc or inhouse with the KAPA Mouse Genotyping Kit (Kapabiosystems, #KK7301). The generation of conditional *Smo* mice has been previously described (Briggs et al., 2016), and their genotyping was conducted with the following primers: the forward: 5′-GAAAGCTGGCCCCAGACTTTCG and reverse: 5′-AGTACCAGCAG-CAGCAACTGC. Generation and genotyping of conditional *Ift88* and *Dzip1* have been previously described (Toomer et al., 2019a; Haycraft et al., 2007). *WT1-Cre/ROSA-eGFP*, *Tie2-Cre*, *NfatC1-Cre, and Nfat-C1-enCre* lines were genotyped as previously described (Toomer et al., 2019a; Wessels et al., 2012). *Dhh* global null mice and conditional flox alleles were previously described (Bitgood et al., 1996)' (Caradu et al., 2018). The forward primer for inhouse *Dhh* floxed allele genotyping was: 5′-TGGGTGTTCCTTACAATCCGC-3’. The reverse primer for inhouse *Dhh* genotyping was: 5′-CAACCACTGGACCGAAGGAGGAA-3’. The forward delta primer was: 5′-TACGGTTCTCTCTGATTGTGATGAGGTC-3′, and the reverse delta primer was: 5′-CAACCACTGGACCGAAGGAGGAA-3’.

Immunohistochemistry and fluorescence imaging. Immunohistochemical and fluorescence stains were performed on 5 μm, paraffin-embedded sections from E10.5, E13.5, E14.5, E15.5, E16.5, P0, and adult wild-type (6-month) and conditional *Dhh* mice as previously described (Toomer et al., 2017, 2019a, 2019b; Durst et al., 2015; Fulmer et al., 2019; Sauls et al., 2015). Primary antibodies and their dilutions included: acetylated tubulin (Sigma, #T6793, 1:500), alpha-smooth muscle actin (Sigma, #A2547, 1:500), alpha-smooth muscle actin (Cell Signaling, #19245, 1:500), ARL13B (Protein Tech, #17711-1-AP, 1:500), Collagen Telo (a generous gift from Dr. Stanley Hoffman, 1:250), DHH (Santa Cruz, #sc-271168, 1:50), Elastin (Abcam, #ab77804, 1:250), Smoothened (Novus, #NSL2666, 1:100), Versican (a generous gift from Dr. Stanley Hoffman, 1:250). Secondary antibodies were all purchased from Invitrogen, used at a 1:100 dilution, and included fluorophores 488, 568, and Cy5. Nuclei were stained with Hoechst (Life Technologies, #H3569, 1:10,000). Slides were cover-slipped using Invitrogen SlowFade Gold Antifade Reagent (#S36936). Images were captured using: Leica TCS SP5 AOBS Confocal Microscope System and LAS AF v2.6.3 Build 8173 Acquisition and Analysis Software, Zeiss Axioscope M2, or Olympus BH-2 brightfield microscope. n > 3/genotype.

3D reconstructions and morphometrics. 3D reconstructions were generated from H&E images as previously described (Toomer et al., 2017, 2019a; Durst et al., 2015; Fulmer et al., 2019) from P0 neonatal mice with the following genotypes: $NfatC1^{enCre(+)};Dhh^{f/f}$ (n = 5), $NfatC1^{Cre(+)};Dhh^{f/f}$ (n = 4), $Tie2^{Cre(+)};Dhh^{f/f}$ (n = 5). Littermate controls were used as comparisons for phenotypic measurements (n = 4 controls for each cKO group). Valve volumes were quantified with Imaris 9.2 software from the rendered 3D reconstruction. Length and thickness measurements were taken from the H&E images with Fiji (Image J) measuring tools. Length was measured along the entire vertical axis of each leaflet from the beginning, middle, and end of the valve. Thickness was measured in 3–4 evenly spaced intervals along the leaflet length to account for overall thickness from the leaflet hinge to tip. Each thickness measurement was taken across the horizontal axis on each 5μm section of each leaflet of the valve. 3D reconstruction of IHC's from valves were created from high-resolution confocal z-stacks using the Imaris 9.2 software.

Movats pentachrome staining. Movats staining was performed on 5μm

sections of wildtype, globally ablated *Dhh*, and *Dhh* conditional knockout (*NfatC1*$^{enCre(+)}$;*Dhh*$^{f/f}$) adult mitral valve tissue. Tissue sections were deparaffinized with xylenes and hydrated through graded ethanol to distilled water. Sections were incubated in Bouin's Fluid at 60 °C for 1 h. This was followed by a 5-min wash in running water and a 20-min incubation in 1% alcian blue at room temperature. Slides were then dipped 5 times in de-ioinzed water and incubated in alkaline alcohol for 10 min at 56 °C. This was followed by a 2-min wash in running water and a 15-min room temperature incubation in Orcein-Verhoeff stain (0.2% Orcein, 5% alcoholic hematoxylin, 10% ferric chloride, 12% Lugol's iodine). Slides were washed for 3 min in running water and stained with wood-stain scarlet-acid fuchsin for 2 min and 30 s. This was followed by incubations in 0.5% acetic acid (30 s), 5% phosphotungstic acid (9 min), 0.5% acetic acid (30 s), and 3 times in 100% EtOH (1 min each). Slides were then incubated in alcoholic saffron for 20 min at room temperature. Finally, slides were dehydrated using two 5-min incubations in 100% EtOH and three 5-min incubations in xylenes and were coverslipped with Cytoseal. n = 3/genotype.

Western blotting. All Western blots were performed in a Bio-Rad mini blot electrophoresis chamber with semi-dry transfer in a Bio-Rad Trans-blot Turbo Transfer system. Protein samples were prepared using a 2x SDS Laemmli buffer (125mM Tris pH7, 10% Glycerol, 2% SDS, 5% β-mercaptoethanol, and .05% bromophenol blue) and boiled at 98 °C for 5 min prior to loading. Proteins were separated in 4–20% Mini-PROTEAN TGX Stain-Free Protein Gels (Bio-rad, #456–8093) and transferred to Trans-Blot Turbo Mini Nitrocellulose Transfer Packs (Bio-rad, #170–4158). Membranes were blocked in 5% nonfat milk (Bio-rad, #170–6404) diluted in 1X Tris Buffered Saline, 0.1% Tween 20 (TBST) for 1 h and incubated in primary antibodies at 4 °C overnight with rotation. The next morning the membranes were rinsed 5 times with TBST and incubated at room temperature for 1 h in secondary antibody. The membranes were then rinsed 5 times in TBST for 10 min each and imaged on a Bio-Rad ChemiDoc MP system with SuperSignal West Femto Maximum Sensitivity Substrate (ThermoFisher, #34096) or Pierce ECL Western Blotting Substrate (ThermoFisher, #32209) as appropriate. Primary antibodies and their dilutions included: GLI3 (Origene, #TA337186, 1:1000), RAC1 monoclonal antibody (Cytoskeleton Inc., #ARC03, 1:500) and Smoothened (GeneTex, #GTX60154, 1:1000). All secondary antibodies were purchased from Sigma and were used at 1:7500. These included: Anti-mouse IgG HRP antibody (#A9044) and Anti-rabbit IgG HRP antibody (#A9169).

Cell density studies. Cell density was quantified as previously described (Toomer et al., 2019a; Fulmer et al., 2019). Total cell numbers were counted using the open-source software, Cellprofiler. A pipeline was created to generate binary images from edited H&E images containing only the valve leaflets to count nuclei per section.

Chicken valve dissection/cell culture/treatment groups. Eggs were purchased from Charles River Labs (#10100326) and incubated in a rotating egg incubator at 37 °C with 55% humidity until Hamburger Hamilton Stage 30–31 (HH30-31), a stage of active valve remodeling. Embryos were then removed from the shell, and the mitral valves were dissected from the heart and stored in sterile PBS until all eggs were dissected. Mitral valves were pooled, and cells were dissociated with Trypsin containing EDTA (Corning, #25-053-CL). Cells were cultured in 100 mm dishes from Sigma (#93100), and maintained in M199 medium (Hyclone, #SH30253.01) supplemented with 5% heat-inactivated chicken serum (Bioworld, #30611183–1), 1% Pen-Strep (Life Technologies, 15070–063), and 0.1% Insulin-Transferrin-Selenium (ITS) (Gibco, #41400–045). Treatment groups for cell experiments included: Untreated, DHH 1μg/ml of recombinant mouse DHH C23II N-Terminus ligand (Novus Biologicals, #NBP2-35175), Antibodies (0.5μg/ml) against SHH (Santa Cruz, #sc-365112), IHH (Santa Cruz, #sc-166685), and DHH (Santa Cruz, #sc-271168), Cyclopamine 25μM (Tocris, #1623), and Cytochalasin D 1μM (Sigma, #C8273). All treatments, unless otherwise specified, were performed in low serum containing media: M199, 0.1% chicken serum, 0.1% ITS, 1% Pen-Strep.

Hydrogel Remodeling assay. Collagen hydrogels were made with serum-free M199 media (Hyclone, #SH30253.01) and 1.5mg/ml Rat Tail Collagen I (Corning, #354236). Fetal chick mitral valve interstitial cells (cVICs) (stage HH30-31) were added to the M199/Collagen mixture after it was neutralized with 1N NaOH at a concentration of $3x10^5$ cells per hydrogel. 400 μl of cell/hydrogel mixture was added to each well of a 4-well plate (Thermo Scientific, #176740) and allowed to polymerize at 37 °C for approximately 1 h. After hydrogels solidified, 500μl of chick valve culture media was added to the top of the gels without detaching them and then incubated overnight at 37 °C. The next morning, the culture media was aspirated and the gels were rinsed twice with sterile 1X Phosphate Buffered Saline (PBS). Treatments were then added in low serum containing media and hydrogels were detached from the well walls with a sterile pipette tip. Gels were imaged every hour for 8 h and again at 24 h (timepoints: 1, 2, 3, 4, 5, 6, 7, 8 and 24 h). Following compaction, hydrogels were collected and embedded in paraffin for sectioning and immunostaining. The hydrogel assay for Supplementary Fig. 8 was conducted in the same manner with the exception of using serum free media containing 1% Pen-Strep and 0.1% ITS during treatment. n = 4 hydrogels/treatment group.

Immunocytochemistry. cVICs were seeded into 4-well, collagen-coated chamber slides and cultured with normal media at 37 °C for 16 h. Cells were serum starved for 5 h and treated in serum free media for 2 h. Media was aspirated and cells were fixed in 4% paraformaldehyde (PFA) for 15 min and permeabilized in 0.1% Triton-X for 5 min. Fixed cells were washed twice in PBS and blocked with 1% bovine serum albumin (BSA) in PBS for 1 h at room temperature. Cells were incubated in primary antibody diluted in 1% BSA for 16 h at 4 °C or 1.5 h at room temperature as necessary, washed twice with PBS and incubated in secondary antibody for 1 h at room temperature. Slides were washed three times for 5 min in PBS, including a wash step with Hoechst (Life Technologies, #H3569, 1:10,000). Slides were coverslipped with Invitrogen SlowFade Gold Antifade Reagent (#S36936). Primary antibodies and their dilutions included: acetylated tubulin (Sigma, #T6793, 1:500), alpha-smooth muscle actin (Sigma, #A2547, 1:500), Collagen Telo (a generous gift from Dr. Stanley Hoffman, 1:250). Secondary antibodies were purchased from Invitrogen, used at a 1:100 dilution, and included fluorophores 488, 568, and Cy5. n = 4 slide chambers/treatment group.

Co-immunoprecipitation. cVICs were cultured as described above, serum starved for 5 h and treated for 1 h in the respective treatment groups. Cell lysates were collected with non-ionic lysis buffer (25mM Tris pH7.4, 150mM NaCl, 1% Igepal, 5% Glycerol) containing 1X protease and phosphatase inhibitor cocktail (Thermo Fisher Scientific, #1861281), snap frozen with liquid nitrogen, and then stored at −80 °C until ready for use. Equal amounts of protein (300μg/sample) were then loaded into 1.5ml tubes with 20ul of A/G agarose beads (50% agarose, Pierce, #20421) and volumes were equalized to 1ml with lysis buffer. Samples were rotated at 4 °C for 30 min to pre-clear the lysates. After centrifugation to pellet the beads, the supernatant was collected and split between two tubes for the co-IP. One tube contained 10 μl A/G agarose beads with 3μl normal mouse IgG (400μg/ml, Santa Cruz, #sc-2025) and the other contained 10μl of agarose beads conjugated to TIAM1 antibody (500μg/ml, 25% agarose, Santa Cruz, #sc-393315 AC). Samples were rotated for 16 h at 4 °C. Supernatant was removed and beads were washed 6 times with 500μl of lysis buffer containing protease inhibitor. Each wash step included centrifuging to pellet the beads for 2 min at 14,000×*g* and rotating the beads for 5 min at 4 °C. All supernatant was removed to leave dry beads. Protein was then eluted at 98 °C for 5 min in 15μl 2x SDS laemmli buffer (125mM Tris pH7, 10% Glycerol, 2% SDS, 5% β-mercaptoethanol, and .05% bromophenol blue diluted in H_20), and used for Western blot analysis. n = 4 samples/treatment group.

RAC1 Activation Assay. RAC1 activation was performed on HH 30 chicken VICs per manufacturers recommendations (Cytoskeleton, Inc., #BK035). Serum starved VICs were treated with 1μg/ml of recombinant mouse DHH C23II N-Terminus ligand (Novus Biologicals, NBP2-35175) for 5, 10, 15, and 30 min. Proteins were isolated from treated and

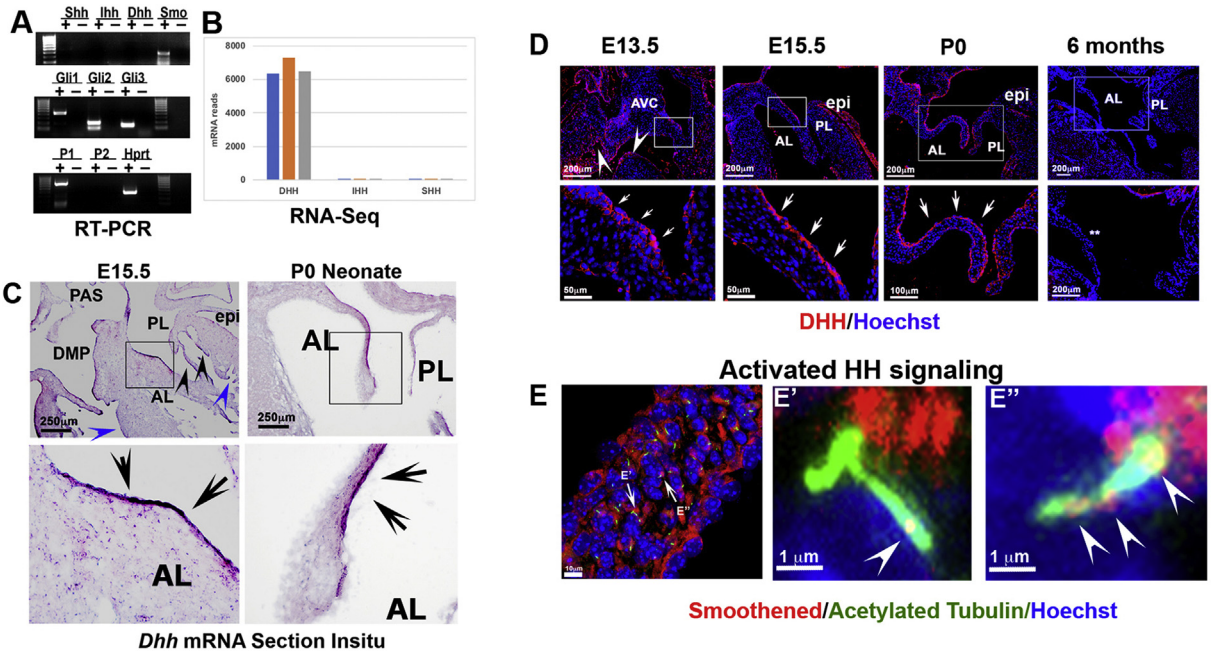

Fig. 1. DHH ligand is expressed by the endocardium and activates Smoothened ciliary translocation in interstitial cells (A) RT-PCR analyses of cultured murine VICs showing expression of *Smo, Gli1, Gli2, Gli3* and *Patched 1* (P1) but not *Shh, Ihh,* or *Dhh*. *Hprt* was used as a control for the RT reaction. **(B)** mRNA reads from RNAseq datasets of isolated anterior mitral valve leaflets at P0 showing *Dhh* is the only hedgehog ligand present within the mitral valves. **(C)** Section in situ for *Dhh* mRNA at E15.5 and P0 showing expression in valve endocardium (arrows), primary atrial septum (PAS), epicardium (epi), ventricular endothelium (blue arrowheads) and endothelium of forming chordae tendineae (black arrowheads). **(D)** IHC shows the expression of DHH protein by endocardial cells of the developing mitral valve (white arrows), epicardium (epi) and ventricular endothelium (white arrows). Expression within the valve is more concentrated along the atrialis. No discernible expression is observed at adult timepoint (**). **(E)** High resolution confocal microscopy and 3D reconstruction of IHC of the anterior leaflet of P0 mitral valves show Smoothened (red) translocation onto ciliary axoneme (green-acetylated tubulin) indicating active HH signaling (arrowheads). AVC = atrioventricular cushion, AL = anterior leaflet, PL = posterior leaflet.

untreated control cells with kit buffers as indicated by instructions. n = 4 replicates.

Statistical analysis. Unless otherwise stated, all error bars are shown as means ± SD. To detect statistically significant differences between groups/genotypes, a Student's t-test was used. P-values are listed in the figure legend for each image. Graphs were generated by SPSS v24 or Excel. Boxplots depict data quartiles and the error bars on these graphs represent the 95% confidence interval.

Animal approval. All experiments on mice were approved by the Institutional Animal Care and Use Committee (IACUC) of the Medical University of South Carolina.

3. Results

3.1. DHH ligand is developmentally expressed by valve endocardial cells and correlates with translocation of smoothened protein on valve interstitial cell axonemes

RT-PCR was performed to assay the presence for hedgehog (HH) ligands and signaling responders in mouse VICs. HH ligands, Sonic (SHH), Indian (IHH), or Desert (DHH) were below the level of detection indicating very low to no expression within this valve interstitial cell line. HH responders: Smoothened (SMO), Patched1 (P1), and the downstream GLI transcription factors (GLI1, GLI2, GLI3) were, however, expressed by this cell population (Fig. 1A). Three independent RNAseq analyses from isolated, individual P0 neonatal mitral valves identified significant levels of mRNA reads for *Dhh*, but no transcripts were detected for *Shh* or *Ihh* (Fig. 1B). These data suggest that *Dhh* is the only hedgehog ligand present within the valves, but is not expressed in valve mesenchyme. To test whether *Dhh* is expressed by valve endocardial cells, section in situ hybridization was performed. As shown in Fig. 1C, *Dhh* is expressed primarily within the valve endocardium at E15.5 with lower levels of expression within the trabeculated endothelium, primary atrial septum and epicardium. By the P0 neonatal timepoint, valvular *Dhh* mRNA expression shows regionalization within the mitral leaflet and is primarily restricted to the atrialis endocardium. Immunohistochemistry (IHC) confirmed the presence of DHH protein within the valve endocardium at embryonic, fetal and neonatal timepoints with evidence of protein diffusion into the interstitium (Fig. 1D). Similar to the mRNA expression, DHH protein is primarily evident within the atrialis aspect of the anterior and posterior mitral leaflets with the highest signal present at the valve tip (Fig. 1D and Supplemental Fig. 1A). Expression of DHH protein was not detected in the adult mitral leaflets (Fig. 1D), indicating a likely developmental role for this growth factor. To test whether hedgehog signaling was active in the valve interstitium, IHC was performed for axonemes and the G-protein coupled receptor (GPCR), Smoothened. In the presence of HH ligand, Smoothened is released from the membrane and travels into the primary cilium (Lum and Beachy, 2004; Lum et al., 2003). Thus, localization of Smoothened serves as a surrogate for hedgehog signaling. Using high resolution confocal microscopy, Smoothened was found both at the ciliary base and within the axoneme, strongly supporting active HH signaling with the valve. In addition, Smoothened staining was also observed in cytosolic regions and in cell types (valve endocardium) that are not associated with the primary cilia, suggesting a cilia-independent role consistent with previous reports (Fig. 1E, Supplemental Fig. 2.) Taken together, our RNA and protein expression studies support a paracrine cross-talk hypothesis in which valve endocardial-produced DHH communicates with valve interstitial cells (VICs) to cause smoothened translocation into the primary cilia to activate hedgehog signaling.

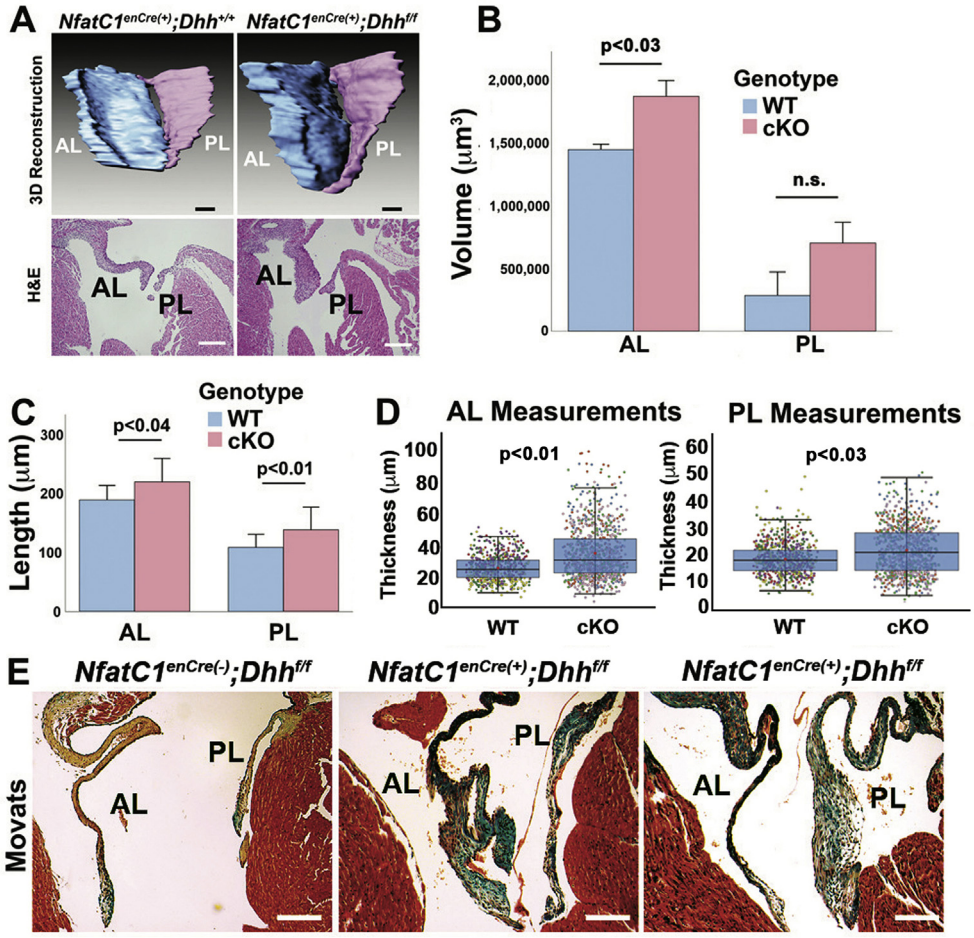

Fig. 2. DHH signals through a paracrine mechanism and its loss results in myxomatous degeneration. (A) 3D reconstructions of P0 mitral valves (top row) created from H&E images (bottom row) showed that conditional knockout of *Dhh* from endocardial cells (*NfatC1*$^{enCre(+)}$;*Dhh*$^{f/f}$) resulted in enlarged valves compared to controls. AL, PL = anterior and posterior leaflets, respectively. **(B)** Quantification of mitral valve volumes from panel A revealed a statistically significant increase in conditional knockout (cKO) volume compared to controls (WT). **(C)** The length of both the anterior and posterior leaflets were significantly increased in cKOs compared to WT. **(D)** Box plots of mitral valve thickness values between wild type and cKO. The blue boxes show the main distribution of the thickness values. The bottom of the box is the 25th percentile, the middle line is the median value, and the top of the box is the 75th percentile. Red dot denotes the mean thickness measurement. Conditional knockouts (cKO) showed an increased range of thicknesses in both anterior and posterior leaflets, and the average thickness was statistically increased in both leaflets compared to controls. Each dot is an individual thickness measurement and the different colors correspond to measurements taken from individual mice. n = 5 animals/genotype. **(E)** Adult *Dhh* conditional knockout mice (*NfatC1*$^{en\text{-}Cre(+)}$;*Dhh*$^{f/f}$) and control littermates were stained for Movats Pentachrome (proteoglycans (blue), collagen (yellow), nuclei & elastin (black), muscle (red), and fibrin (bright red)). *NfatC1*$^{enCre(+)}$;*Dhh*$^{f/f}$ mice showed enlarged anterior (AL) and posterior (PL) leaflets with blurring of molecular boundaries, increased proteoglycans and enlarged/redundant valve tissue compared to controls, indicating a myxomatous phenotype.

3.2. Genetic depletion of Dhh in the valve endocardium results in abnormal valve morphogenesis and adult myxomatous mitral valves

DHH conditional mice (*Dhh*$^{f/f}$) were used (Caradu et al., 2018) to assay the cell-specific function of DHH during valve development and to validate the DHH antibody (Supplemental Fig. 1). We initially examined *Dhh*$^{f/f}$ mice maintained on either the *Tie2*^{Cre} or *NfatC1*^{Cre} backgrounds. Both of these Cre lines genetically remove *Dhh* in endothelial and endothelial-derived cells. As the mitral valves are initially built through an endothelial-to-mesenchymal transformation (EndoMT), these Cre lines will remove *Dhh* from a majority of cells that make up the mitral valves in its entirety. Although subtle phenotypic differences were observed between each of these Cre-lines, the mitral leaflets from both lines displayed quantifiably altered valve morphology in both length and thickness (Supplemental Fig. 3). In all animals examined, the valves exhibited regional thickness, width and length alterations, resulting in enlarged valve leaflets at P0. To test whether the DHH signal emanating from the endocardium is responsible for regulating valve morphogenesis as suggested by its expression pattern (Fig. 1A–D), *Dhh* floxed mice were bred onto the *NfatC1*$^{enCre(+)}$. This Cre is specifically expressed in valve endocardial cells that do not undergo EMT and thus, enables deletion of *Dhh* only in the valve endocardium (Wu et al., 2011). Depletion of *Dhh* in valve endocardial cells resulted in a mitral valve phenotype similar to the *Tie2*^{Cre};*Dhh*$^{f/f}$ and *NfatC1*^{Cre};*Dhh*$^{f/f}$ mice. Morphometric analyses of 3D reconstructions and measurements obtained from H&E sections demonstrated that mitral valve leaflets in the *NfatC1*$^{en\text{-}Cre(+)}$;*Dhh*$^{f/f}$ mice had abnormal valve morphology with significant increases in volume, length and thickness measurements at the neonatal P0 timepoint (Fig. 2A–D). Consistent with our previous reports, we also observed a 50% (3 out of 6) penetrant right-noncoronary BAV phenotype in these mice (Supplemental Fig. 4). We observed no significant changes in cilia length on valve interstitial cells (Supplemental Fig. 5), demonstrating that loss of Dhh does not impair ciliogenesis.

To define whether loss of *Dhh* could result in a myxomatous valve as seen in patients with MVP, adult *NfatC1*$^{en\text{-}Cre(+)}$;*Dhh*$^{f/f}$ adult mice were examined histologically by Movats Pentachrome stains. As shown in Fig. 2E, developmental depletion of *Dhh* in the valve endocardium resulted in adult myxomatous anterior and posterior leaflets in 100% of animals examined. This phenotype was consistent with the myxomatous valves observed in global *Dhh* deletion adult animals (Supplemental Fig. 6). Both global and conditional knockout models for *Dhh* exhibit excess leaflet tissue and have disrupted ECM boundaries including loss of fibrillar collagen and increased proteoglycans and elastin.

3.3. Cilia do not regulate canonical hedgehog signaling in the mitral valves

To begin exploring the mechanisms by which DHH signaling through primary cilia can regulate valve development and lead to myxomatous

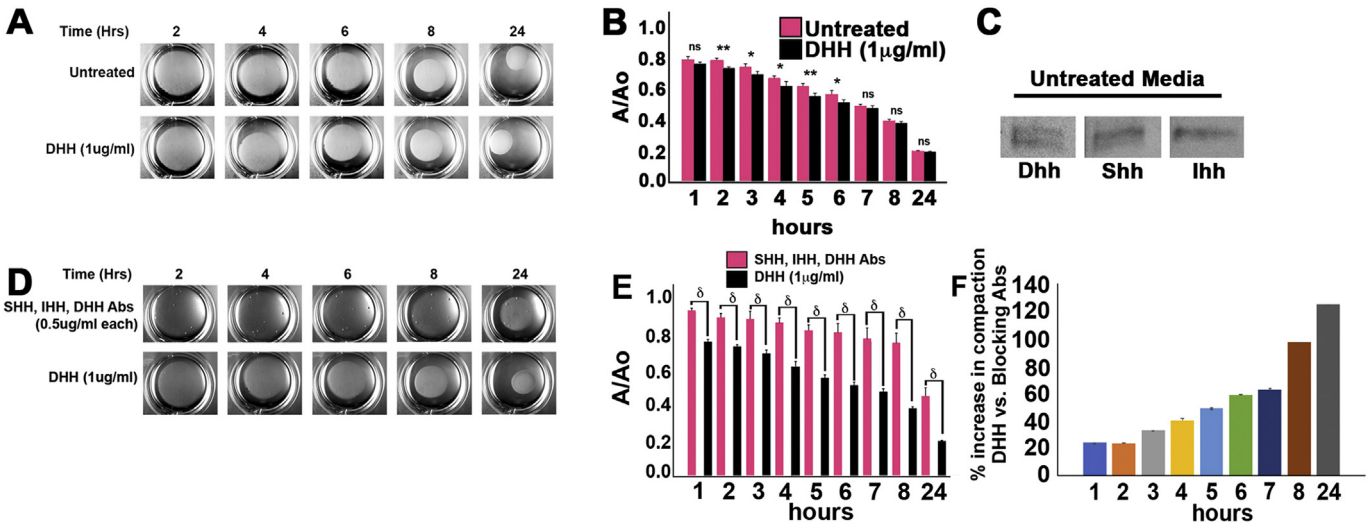

Fig. 3. DHH treatment promotes VIC contraction in 3D collagen hydrogel *in vitro* assays. (A) Representative images of Untreated and DHH treated hydrogels seeded with embryonic chicken VICs (cVICs, HH30-31) over the course of 24 h. **(B)** Graph of hydrogel diameter change from (panel A) over time shows DHH treatment increased hydrogel contraction from hours 2–6 compared to control, but there was no statistical (n.s.) difference by 24 h ns = not significant, * = $p < 0.05$, ** = $p < 0.005$ **(C)** Westerns revealed that HH ligands were present in serum samples from untreated media. **(D)** Antibodies against HH ligands blunted compaction of collagen gels compared to the DHH treated group. **(E)** Quantification of hydrogel diameters from panel D showed antibodies against HH ligands significantly reduced contraction rate compared DHH treatment. δ = $p < 0.0005$ **(F)** Quantification of percent increase in compaction compared between DHH stimulated and antibody treated showing that over time, DHH treated gels compact significantly more at every timepoint evaluated.

valves later in life, we initially examined whether canonical hedgehog signaling is impacted by primary cilia. Following a hedgehog signal through the primary cilium, GLI3 is cleaved into activator and/or repressor transcription factors (Dai et al., 1999; Sasaki et al., 1999; Wang et al., 2000). Thus, the ratios of GLI3 activator vs repressor are well established readouts for active hedgehog signaling through the primary cilium. In our study, isolated mitral valves from two independent models of cilia deficiency (*Ift88* and *Dzip1*), were assayed by Western analyses for differences in these cleavage products (Supplemental Fig. 7). Western analyses of isolated mitral leaflets from wildtype, conditional heterozygote, and knockout mice revealed no statistically significant change in the ratio's between full length (GLI3 transcriptional activator) or GLI3 repressor (Supplemental Fig. 7A and B). As transcription of GLI factors and Patched1 is under the control of GLI transcription regulators through an autocrine feedback loop, we examined whether mRNA of *Gli1*, *Gli2*, *Gli3* and *Patched 1* was changed as a global readout for altered canonical hedgehog signaling in the valves. In mitral leaflets isolated from cilia-deficient *Dzip1* and *Ift88* conditional knockout mice, no statistically significant change in mRNA levels for these *Gli* transcriptional targets were observed (Supplemental Fig. 7C). Although *Gli* transcription factor mRNAs are expressed by mitral VICs, our data suggest that canonical hedgehog signaling does not impact GLI cleavage or transcription and thus, are unlikely to contribute to disease phenotype.

3.4. Desert hedgehog functions through a non-canonical pathway to remodel the cytoskeleton

There are currently two known non-canonical signaling pathways in which hedgehog can function. The first (type I) pathway results in increased proliferation. However, previous reports have shown that loss of cilia either through *Ift88* or *Dzip1* deletion in the valves does not result in a significant change in proliferation (Toomer et al., 2017, 2019a). Consistent with these prior reports, we do not see a change in total cell number in the *Dhh* conditional knockout mitral leaflets (Supplemental Fig. 8A–C) compared to control littermates. These data suggest that DHH signaling and/or primary cilia have little impact on cell proliferation during valve morphogenesis and type I noncanonical signaling is not likely impacting valve development. The second (type II) non-canonical hedgehog pathway involves cytoskeletal remodeling (Chinchilla et al., 2010). During mitral valve development, VICs reorganize/activate their cytoskeleton and become aligned within the tissue (Durst et al., 2015; de Vlaming et al., 2012; Butcher and Markwald, 2007; Gould et al., 2016). As a consequence, the ECM, which is attached to the cells also becomes aligned in a process called “ECM compaction or ECM remodeling”. Thus, we hypothesized that DHH-signaling, through a type II non-canonical mechanism, activates the VIC cytoskeleton and results in ECM compaction, ultimately leading to leaflet attenuation and thinning. We initially tested this by assaying cellular density within the *Dhh* conditional knockout valves. Consistent with our previous findings in the *Ift88* and *Dzip1* conditional knockout mice (Toomer et al., 2017, 2019a; Fulmer et al., 2019), there is a reduction in cell density in the mitral leaflets at P0 (Supplemental Fig. 8A and B) and an increase in extracellular space between cells compared to control littermates. This indicates a potential failure for the cells to actively remodel and condense the surrounding ECM.

To directly test the effect of DHH signaling and the role of primary cilia in ECM remodeling through activation of the cytoskeleton, we employed 3D collagen gel compaction assays. In these assays, cells are embedded within free-floating collagen gels and upon stimulation, will compact the gel over time. These assays are commonly used as an efficient and reproducible method for quantifying cytoskeletal dynamics and ECM compaction *in vitro* (Gould et al., 2016). Embryonic chicken valvular interstitial cells (cVICs) during stages of active valve remodeling (HH30-31) were dissected, cultured, and entombed with collagen hydrogels (1.5mg/ml), released from the side and bottom of the wells and subsequently treated with DHH ligand (mouse C23II, 1μg/ml). While the results showed that DHH treated cells had significantly smaller hydrogel diameters at 2–6 h post treatment, the results were modest and there was no difference in hydrogel compaction after 7 h of treatment (Fig. 3A & B). This prompted us to investigate whether hedgehog ligands were present within the media, potentially masking the effect of exogenously added ligand. Western blotting of unconditioned media confirmed the presence of each of the three hedgehog ligands present within the media (Fig. 3C). To test whether hedgehog ligands were responsible for promoting collagen remodeling in this gel system, antibodies directed against each of the hedgehog ligands were added to the culture media.

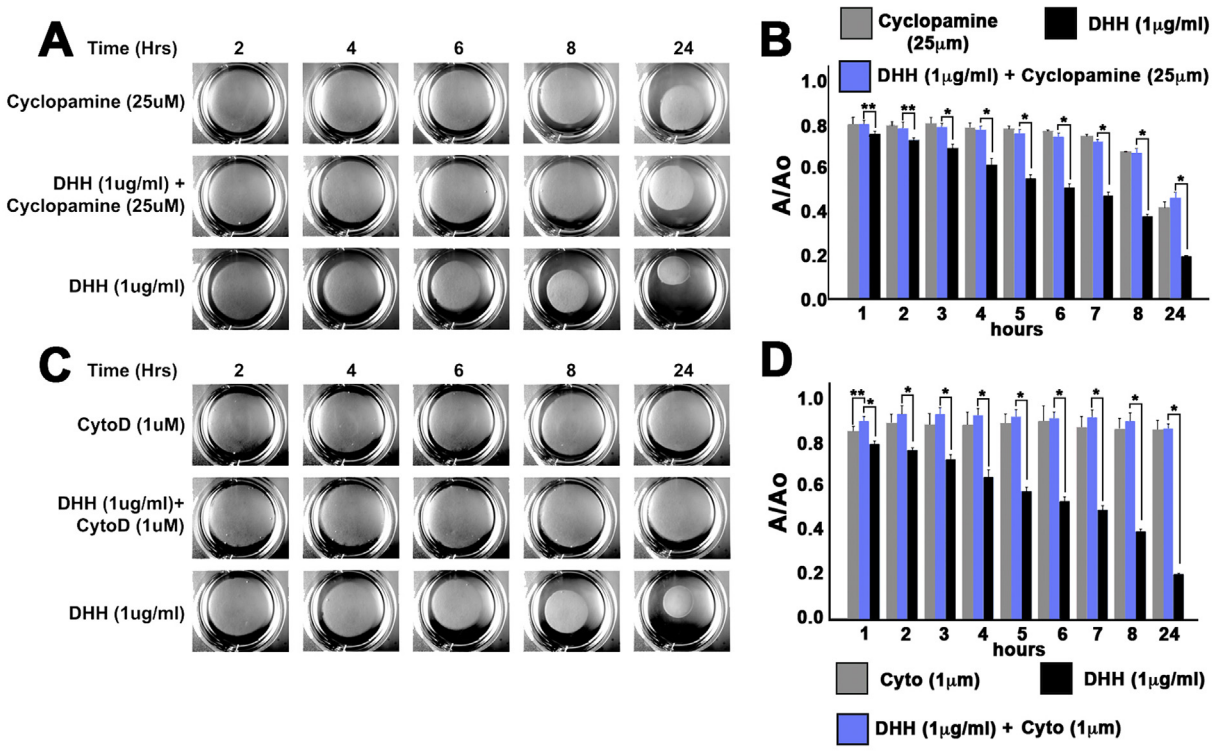

Fig. 4. ECM remodeling is dependent on cilia/smoothened signaling. (A) Cyclopamine, a Smoothened-specific HH inhibitor, reduced hydrogel contraction compared to the DHH treated group. **(B)** Graph depicting the quantification of hydrogels from the groups in panel A. There was no significant difference between cyclopamine alone versus cyclopamine plus DHH ligand. * = $p < 0.05$, ** = $p < 0.005$ **(C)** Treatment with the actin polymerization inhibitor, cytochalasin D (CytoD), prevented hydrogel contraction. **(D)** Quantification of CytoD vs DHH treatment from gels in panel C shows CytoD significantly reduced contraction of hydrogels, demonstrating that collagen remodeling is dependent on an intact and active actin cytoskeleton. * = $p < 0.05$, ** = $p < 0.005$.

Addition of these blocking antibodies significantly impacted the rate of collagen remodeling in the gels at every timepoint investigated (Fig. 3D–F) demonstrating a crucial role for hedgehog signaling in cell-driven ECM compaction. As DHH is the only hedgehog ligand expressed during cardiac valve development, the data strongly support that this growth factor is driving valve ECM compaction. This was further confirmed in serum free media stimulated with DHH ligand. As shown in Supplemental Fig. 9, DHH was sufficient to stimulate robust ECM remodeling by cVICs in our collagen gel cultures.

To test whether DHH signaling is dependent on primary cilia, chicken VICs were treated with cyclopamine (Fig. 4A and B). Cyclopamine is a Hedgehog-specific inhibitor that binds to Smoothened to prevent its signaling through the primary cilium (Taipale et al., 2000). VICs stimulated with cyclopamine (25μm) displayed a pronounced delay in their ability to remodel the collagen ECM compared to control and DHH treated gels. Results from combinatorial treatment of DHH and cyclopamine were similar to those obtained from cyclopamine-only treated gels, suggesting a DHH-dependency on Smoothened at the primary cilium. Cytochalasin D (CytoD), an actin depolymerizing agent was used as a control to validate that gel compaction is due to actin organization. Chicken VICs, that were stimulated with CytoD failed to compact collagen gels over a 24-h timepoint. The addition of DHH to CytoD treated cultures had no impact on the cVICs ability to remodel the ECM as anticipated (Fig. 4C and D). Brightfield images of the hydrogels taken at the 24-h timepoint confirmed that cell viability was likely not a factor in the differences in hydrogel remodeling (Supplementary Fig. 10A). 3D reconstructions of cVICs from the hydrogels also showed that cells treated with DHH exhibited a different pattern of α-SMA staining compared to cyclopamine and CytoD treated cells (Supplementary Fig. 10B). In the cyclopamine treated cultures, the cells exhibited a rounded morphology and perturbed α-SMA organization with no evidence of linearly organized actin filaments. The α-SMA staining in the cytochalasin D treated cells appears jagged and consistent with depolymerized actin cables. Conversely, the DHH treated cells have elongated filopodia with organized actin and appear to make syncytial networks with neighboring cells. These data strongly support DHH as regulating α-SMA organization and ultimately, ECM remodeling, through a Type II (Smoothened-dependent) non-canonical cilia signaling mechanism. Western analyses of these gels revealed no changes in total α-SMA protein amounts, further indicating that cellular distribution and/or organization of a-SMA is driven by DHH signaling (Supplemental Fig. 11).

3.5. Smooth muscle actin organization is regulated by DHH and primary cilia during development in vivo

Our data showing that DHH can regulate α-SMA organization *in vitro*, combined with the observation that DHH and cilia are only present during developmental timepoints *in vivo* indicates that α-SMA activation may represent a unique DHH-driven cell phenotype within the mitral valves during development. Immunohistochemical stains revealed that α-SMA is expressed by VICs within specific regions of the valve during timepoints of active valve remodeling (Fig. 5A). During early stages of valve morphogenesis, α-SMA is not observed in newly transformed mesenchymal cells at E10.5, but is robustly expressed by developing myocytes (Fig. 5A and (Horne et al., 2015)). Within the valves at E13.5, expression of α-SMA is confined to a small group of cells at the junction where superior and inferior AV cushions have fused as well as in a few interstitial cells within the distal regions of the anterior and posterior leaflets (Fig. 5A). By E15.5, expression becomes more pronounced within VICs localized to the distal tips of the mitral leaflets. The expression of α-SMA continues to increase in this region of the leaflet at P0 and correlates with the timepoints of active valve compaction/remodeling, the expression of primary cilia and the presence of DHH protein (Fig. 5B and C and Supplemental Fig. 1). To test whether expression of α-SMA is affected by DHH, we performed IHC and 3D-reconstructions of immunostains throughout the entire valve of control and *NfatC1*$^{Cre(+)}$ mice

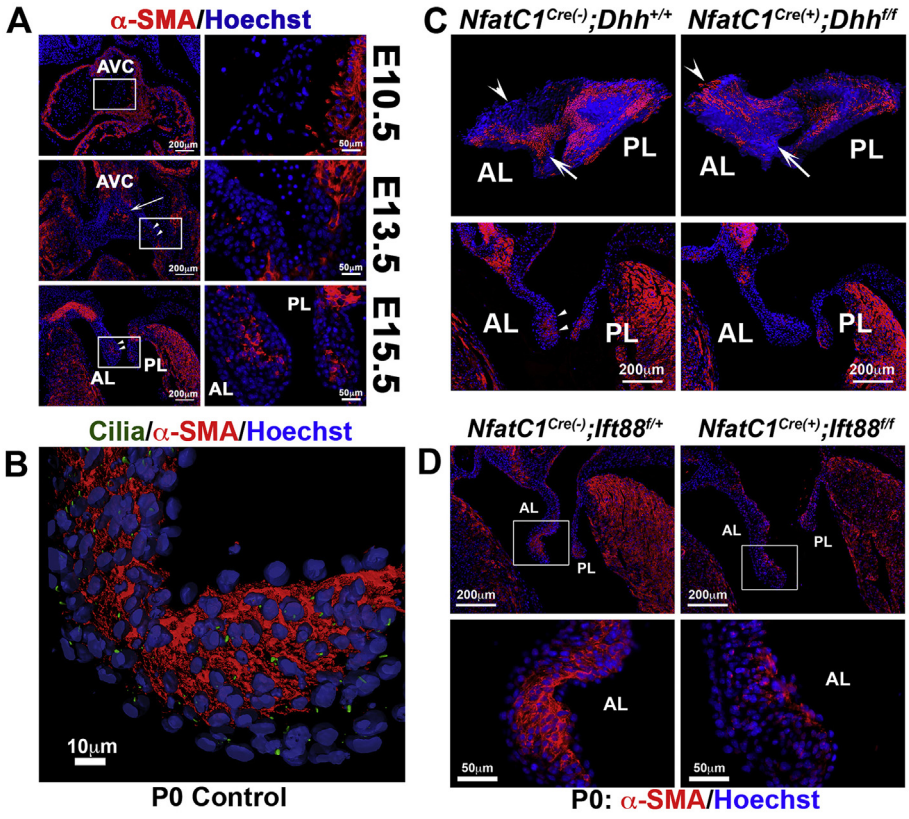

Fig. 5. Temporal-spatial α-SMA is regulated by *Dhh* and primary cilia *in vivo*. **(A)** IHC showed that α-smooth muscle actin begins to be expressed in the atrioventricular cushion (AVC) by E13.5 and continues to increase in later stages of valvulgenesis. α-SMA is robustly expressed within the myocardium at all timepoints analyzed. The expression within the valves is restricted to a core of cells localized to the fusion region of the superior and inferior cushions (arrow) as well as within the tip of the anterior and posterior leaflets (arrowheads). **(B)** 3D reconstruction created from z-stack of high-resolution confocal image of wildtype anterior leaflet shows primary cilia (green) are present throughout α-SMA rich regions (red) within the valve tip. **(C)** 3D reconstruction (top row) of control (*NfatC1*$^{Cre(-)}$;*Dhh*$^{+/+}$) and *Dhh* conditional knockout (*NfatC1*$^{Cre(+)}$;*Dhh*$^{f/f}$) P0 mitral valves show reduced α-SMA (red) expression compared to wildtype controls. White arrow heads indicate areas of high α-SMA expression on the wildtype anterior leaflet on IHC stains from which the 3D reconstructions were created (bottom row). **(D)** Mitral valves of cilia conditional knock outs (*NfatC1*$^{Cre(+)}$;*Ift88*$^{f/f}$) also show an apparent reduction in α-SMA expression (red) compared to controls. AVC = atrioventricular cushion, AL = anterior leaflet, PL = posterior leaflet.

(Fig. 5C and Supplemental Movies 1 and 2). In control mitral leaflets at P0, expression of α-SMA is expressed primarily in regions of apposition between the anterior and posterior mitral leaflets. This pattern of expression was significantly attenuated in the *NfatC1*$^{Cre(+)}$;*Dhh*$^{f/f}$ valves (Fig. 5C, Supplemental Movies 1, 2). Loss of cilia resulted in a similar change in α-SMA expression and its spatial distribution (Fig. 5D).

Supplementary video related to this article can be found at https://doi.org/10.1016/j.ydbio.2020.03.003

In an attempt to identify the tissue layer in which these α-SMA cells reside, IHC co-stains with markers of the fibrosa (collagen 1α1) and spongiosa (versican) were performed and revealed an imperfect overlap between α-SMA expressing cells and either of these markers (Supplemental Figs. 12 and 13). The altered distribution of α-SMA in the conditional heterozygote and knockout correlates with areas of lower versican expression in the valve tips (Supplemental Fig. 12). Although some overlap is evident between collagen and α-SMA expressing cells in control mitral leaflets, this expression is limited to the middle of the mitral tip. The DHH heterozygote and knockout mice fail to show this pattern and the cells that express α-SMA in this region do not appear to appreciably overlap (Supplemental Fig. 13). Loss of one allele of *Dhh* was sufficient to generate these molecular changes indicating that gene dosage of this growth factor is critical. These data suggest that α-SMA positive VICs likely mark a unique sub-population of endothelial-derived cells within the tips of the mitral valves. This hypothesis was further tested by performing IHC on WT-1 lineage traced mice, which labels epicardial-derived cells (EPDCs) (Horne et al., 2015). Consistent with α-SMA marking a novel population of endothelial-derived cells within the mitral leaflet tips, expression is not observed within EPDCs of the anterior or posterior leaflets at P0 (Supplemental Fig. 14).

3.6. *DHH promotes filamentous α-SMA organization through TIAM1 mediated RAC1 activation*

Our data demonstrate a critical role for DHH signaling through the primary cilium in the regulation of collagen gel compaction (Figs. 3 and 4) and α-SMA organization (Fig. 5, Supplemental Fig. 10). Anisotropic filamentous actin is required for force generation and remodeling of ECM (Versaevel et al., 2012; Farsi and Aubin, 1984; D'Addario et al., 2001; D'Addario et al., 2002; D'Addario et al., 2003; Ehrlicher et al., 2011; Sandbo and Dulin, 2011; Lim et al., 2012). Thus, we tested whether DHH could induce organized, anisotropic α-SMA filaments. Immunocytochemistry of unstimulated cVICs in serum-starved cultures revealed prominent α-SMA expression. This expression was primarily restricted to the cell periphery with a notable lack of mature α-SMA filaments (Fig. 6A). Under DHH stimulated conditions, however, we observed a profound increase in anisotropic, α-SMA filaments that were well organized within the VICs (Fig. 6A'). To test if this organization was dependent on active hedgehog signaling, the Smoothened inhibitor, Cyclopamine was used. ICC of cyclopamine-treated cultures revealed a complete loss of filamentous α-SMA staining with no discernible difference in organization between DHH-treated and controls (Fig. 6B, B′). The actin depolymerizing agent, Cytochalasin D gave a similar response with no evidence of mature filamentous α-SMA between DHH-treated and controls (Fig. 6C, C′). These data further demonstrate a role of DHH signaling through the primary cilium in organizing anisotropic α-SMA filaments.

To gain mechanistic insight into how DHH might regulate smooth muscle actin polymerization through the primary cilium, we investigated whether RAC1 activation might be involved. RAC1 is a member of the p21 Rho-family of small GTPases that are master regulators of actin cytoskeletal rearrangements (Chinchilla et al., 2010; Gould et al., 2016; Duval et al., 2014). Recent data has demonstrated that RAC1 is activated by the small GEF, TIAM1 (T cell lymphoma Invasion and Metastasis) (Sasaki et al., 2010). As TIAM1 has been shown to interact with Smoothened and upon hedgehog stimulation (Sasaki et al., 2010), function as a GEF for RAC1 to polymerize actin, we initially tested by Co-immunoprecipitation (Co-IP) whether this interaction was functioning in our culture models (Fig. 6D). In full serum containing media (containing each hedgehog ligand and/or spiked with additional DHH protein), we detected no appreciable interaction between TIAM1 and

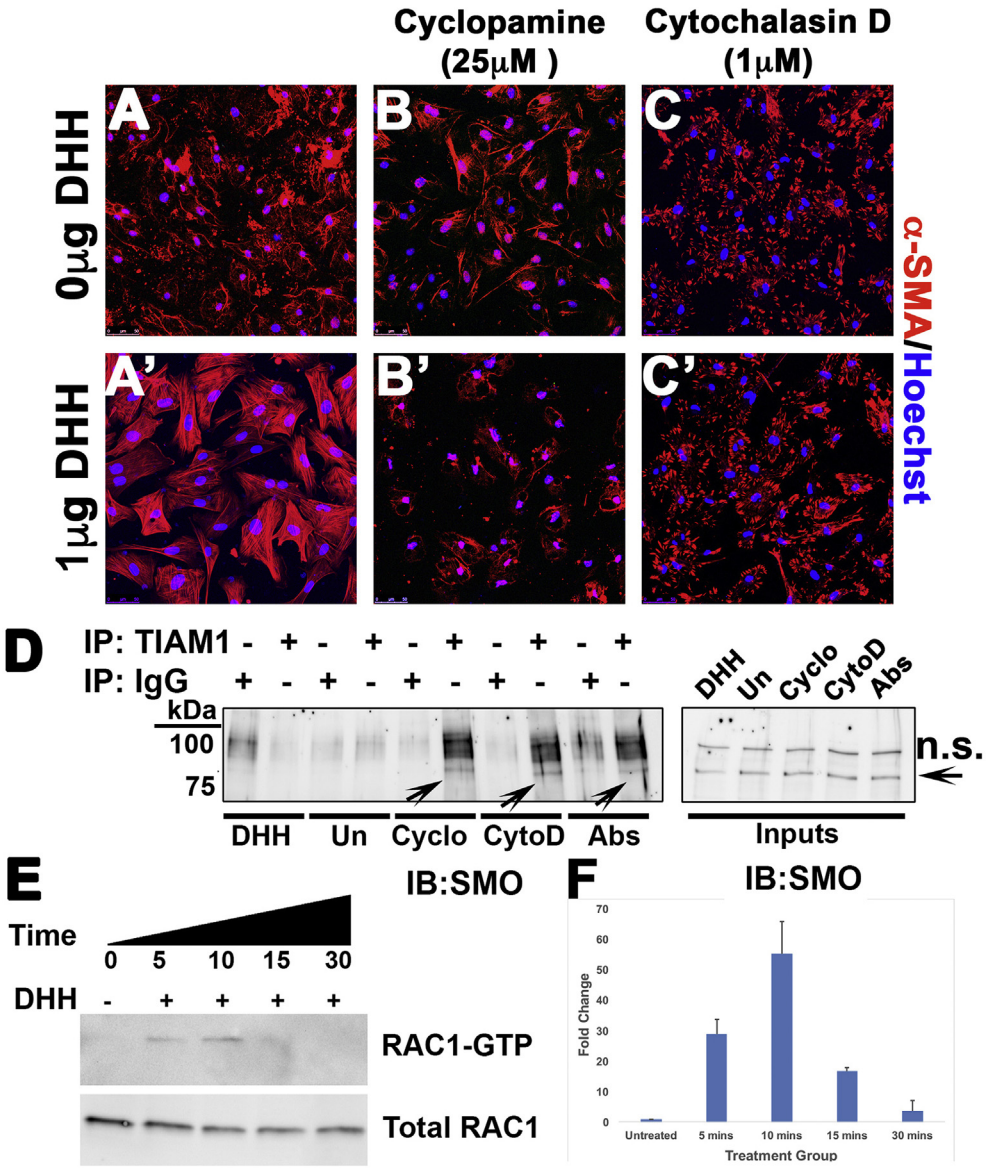

Fig. 6. DHH stimulates α-SMA organization through a Smoothened-dependent TIAM1-RAC1 activation. (A, A′) Serum starved cVICs (HH30-31) display α-SMA expression along the cell periphery. Addition of DHH (1μg/ml) to cVICs induces a rapid reorganization of α-SMA stress fibers. **(B,B′)** Addition of the smoothened inhibitor completely blocks this DHH-mediated actin effect as does depolymerization of the smooth muscle actin cytoskeleton with cytochalasin D **(C,C′).** **(D)** Co-immunoprecipitation showed that HH treatment from DHH ligand or HH-containing untreated media results in the loss of Smoothened (SMO) and TIAM1 binding. This effect is inhibited by cyclopamine (Cyclo), cytochalasin D (CytoD), or HH antibodies (Abs). Inputs for each of the co-IP experiments are shown to the right and display relatively equal presence of smoothened protein in the lysate **(E)** DHH treatment activates the TIAM1 target kinase RAC1 (RAC1-GTP) in cVICs, inducing a greater than 50-fold increase within 10 min.

Smoothened. However, following treatment of the cultures with antibodies against each of the hedgehog ligands to block receptor-ligand interactions, TIAM1 was observed as interacting with Smoothened (Fig. 6D). This indicated that presence of hedgehog ligand resulted in a disruption of the TIAM1-Smoothened interaction. Similarly, cyclopamine, which binds to Smoothened and induces an inactive confirmation of Smoothened, resulted in retention of a Smoothened-TIAM1 interaction by Co-IP (Fig. 6D). Treatment with the actin depolymerizing agent, cytochalasin D also led to an interaction between TIAM1 and Smoothened (Fig. 6D). These data suggested that DHH is required for the release of a TIAM1-Smoothened interaction, coincident with smooth muscle actin polymerization. As free TIAM1 is a GEF for RAC1, we tested whether DHH treatment of serum starved cultures could result in an increase in RAC1 activation as assayed by RAC1-GTP levels. Consistent with this hypothesis, stimulation of serum-starved cVICs with DHH resulted in a dose-dependent increase in activated RAC1-GTP (Fig. 6E and F). This dependency of RAC1 activation of DHH was further evaluated in the *NfatC1*$^{Cre(+)}$; *Dhh*$^{f/f}$ mitral valves compared to littermate controls. Loss of DHH *in vivo* resulted in a profound loss of activated Rac1-GTP in the valve interstitial cells (Supplemental Fig. 15).

4. Discussion

Mitral valve prolapse is a common disease affecting 2.5% of the general public with a poorly understood etiology. Until recently, studies on MVP have been relegated to end-stage phenotyping. These studies have led to the understanding of the molecular and structural phenotypes of a myxomatous valve (Rabkin et al., 2001; Rabkin-Aikawa et al., 2004; Hjortnaes et al., 2016). In these abnormal, biomechanically inferior tissues, there is very little phenotypic similarity with unaffected valves in terms of their structural organization. The beautifully organized ECM makeup of elastin, proteoglycans and collagen that is observed in normal mitral valves is lost in MVP patients. Blurring of these ECM boundaries in diseased tissues are only one difference. Cell phenotypes are also different between a normal and MVP disease valve with evidence of increased inflammatory cells (Sauls et al., 2015; Hulin et al., 2018), myofibroblasts, robust cellular activities and overall lack of cellular quiescence (Rabkin-Aikawa et al., 2004). How the valve tissue progresses to this stage of disease in a patient with MVP is, however, unknown. Recent genetic discoveries have pointed to aberrant primary cilia as causative to MVP in affected families as well as in the population (Yu

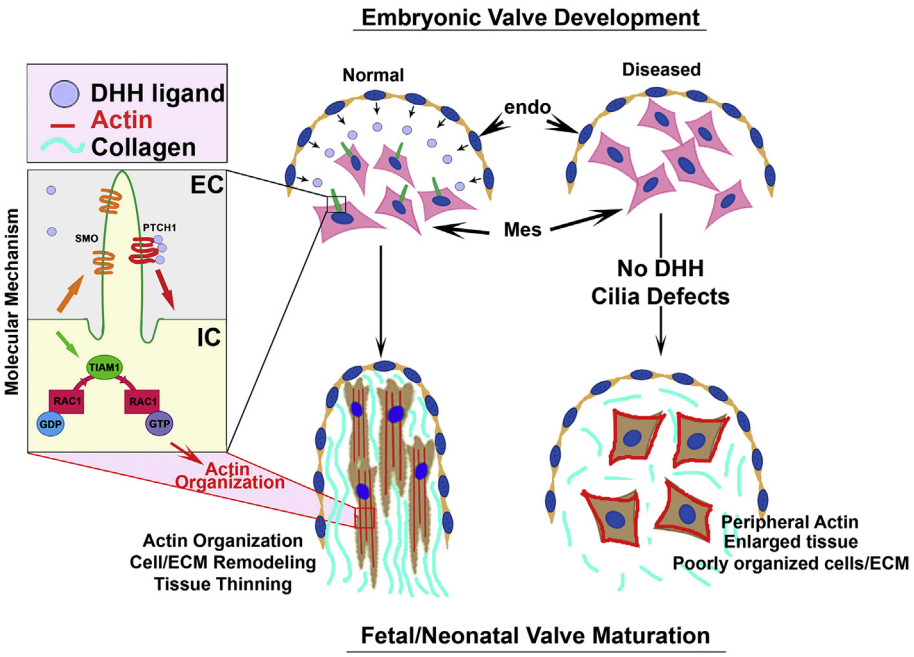

Fig. 7. Model of DHH-cilia signaling in valve development. In normal embryonic valves, the endocardium (endo) releases DHH ligand, which acts on ciliated mesenchyme (mes). Upon binding to patched (PTCH1), smoothened is de-repressed, which leads to TIAM1 activation of RAC1 (RAC1-GTP). RAC1-GTP consequentially activates actin, which promotes its organization, collagen remodeling and tissue thinning and elongation during fetal gestation. In the absence of DHH or in the context of cilia gene variants as seen in patients with MVP, the hedgehog signal is not received, and α-SMA organization fails to occur resulting in a defective valve remodeling and poor cellular and ECM organization.

et al., 2019; Toomer et al., 2019a; Durst et al., 2015; Dina et al., 2015). Uncovering how primary cilia function will likely provide key insight into mechanisms that go awry in MVP patients.

Although it is now clear that primary cilia are required for valve development and can cause myxomatous valve disease and MVP in mouse models and in patients with disease, the function of these cellular antennae in the valves have remained elusive. The classical signaling of hedgehog through the primary cilium to regulate GLI transcription factors is by far the most common mechanism of function. However, it is becoming clear that this signaling cascade, which ends in GLI transcriptional target gene regulation, is far more complex and can function through different mechanisms depending on cell-context. In this study, for example, we found no evidence to support a Hedgehog-cilia-GLI pathway in two independent cilia-deficient genetic models. This contradicts previous reports of *Ift88* (Liu et al., 2005) and *Dzip1* deletion (Wang et al., 2013; Tay et al., 2010; Kim et al., 2010; Wolff et al., 2004; Sekimizu et al., 2004), which showed a profound effect on GLI repressor versus activator forms with consequences on modulation of GLI transcriptional targets. The differences between our study and other previous reports likely reside in the context of the interrogated tissue-type, cell--type and cell-ECM microenvironment. Another main difference may reside in the ligand itself. Whereas most reports focus on sonic hedgehog (SHH) as the major driver of cilia-dependent signaling in most cells within the body, our data do not support a role for SHH in the valves. RNAseq and RT-PCR revealed the presence of *Dhh* mRNA within the developing mitral valves and not *Shh* or *Ihh*. Previous reports have shown that, although the affinity between the hedgehog ligands is similar with Patched, their potencies to stimulate the canonical pathway are very different with a potency of Shh » Ihh » Dhh (Chinchilla et al., 2010). Thus, the decision to function through a canonical (GLI-dependent) or non-canonical pathway likely resides in the type of hedgehog ligand present, concentration gradient within the tissue and diffusivity of the ligand. Our data showing activation of ciliated VIC's in close proximity to the highest degree of DHH expressing endocardial cells lend support to this hypothesis of a limited concentration gradient and/or restricted diffusion rate (Supplemental Fig. 1).

For Hedgehog to function through the primary cilia, it must bind to its cognate receptor, Patched at the ciliary base. This binding induces a conformation change that de-represses Patched inhibition of the GPCR, Smoothened, which then traverses into the ciliary axoneme. Theoretically, knocking out Smoothened should show a similar phenotype in the valves compared to valves in *Ift88*, *Dhh*, and *Dzip1* mouse models. Although previous reports have stated no valve phenotype in the *Tie2*^{Cre};*Smoothened* floxed mouse (Goddeeris et al., 2008), our studies using the *NfatC1*^{Cre} resulted in a robust phenotype (Supplemental Fig. 16). The reason for these differences are unclear but may reside either in the type of Cre used, the degree of persistent smoothened expression in the valves, or technical differences between our imaging modalities.

Within the valves, primary cilia and desert hedgehog are primarily observed during development timepoints. It is becoming recognized that during fetal morphogenesis, cardiac valves need to be reshaped and reorganized to conform to the growing heart and increasing hemodynamic demands. Although still poorly understood, various groups have proposed a need for actin-driven mechanics to reshape the valve (Gould et al., 2016; Butcher et al., 2007a, 2007b; Yalcin et al., 2011). Consistent with this theory, we show that DHH expression is capable of regulating collagen gel remodeling *in vitro*, which is primarily dependent on actin kinetics since dismantling the actin cytoskeleton completely abrogates compaction. Our previous reports on cilia-deficient valves (Toomer et al., 2019a) and our current findings *in vivo* also highlight a function for primary cilia and DHH signaling in the regulation of fetal valve remodeling. Mechanistically, we identified a pathway in which DHH ligand, through the primary cilium could regulate the organization of α-smooth muscle actin, typically viewed as a contractile myofibroblast marker. While, the presence of this gene is commonly associated with end-stage disease phenotypes, it is now clear that this is only a small part of α-SMA's function. In fact, we detect α-SMA protein expression in unique temporal-spatial patterns during valve development. Thus, categorizing α-SMA solely as a myofibroblast marker is not necessarily correct as it is expressed within valve interstitial cells that appear phenotypically identical to their neighboring cells. As α-SMA positive cells do not label exclusively with collagen or proteoglycan markers, respectively, we are unable to characterize them as a specific cell type. As such, our *in vivo* and *in vitro* data suggest that they likely represent a novel DHH-responsive cell type within the tips of the valves. Upon stimulation by DHH, these cells undergo a robust re-organization of the contractile α-SMA cytoskeleton. Genetic perturbation of primary cilia or *Dhh* as well as pharmacological disruption of Smoothened function do not result in a change in α-SMA expression levels (Supplemental Fig. 11), but rather a change in

the distribution and organization of the actin architecture. As we show, this change in α-smooth muscle actin organization can be driven, at least in part, by a complex kinase cascade involving TIAM1 and RAC1.

How organizing the actin cytoskeleton into anisotropic arrays of α-SMA leads to ECM remodeling is not well understood. It is logical to propose that α-SMA organization results in shape changes that establish long, thinned fibroblasts. As these fibroblasts are connected to the ECM via integrins and other receptors, the ECM passively adopts a stratification similar to the cells. In this way, the cellular-ECM syncytium acquire an aligned shape within the valve tissue. With this perspective, stating that α-SMA functions to promote "contraction" of VICs is incorrect and care should be placed on the description of such. Additionally, the presence of bonafide acto-myosin contractile cables within the valve interstitial cells has not yet been fully described, and further questions the contractibility of these cells. Rather, it is more likely that α-SMA induces cell shape changes and the ECM attached to the VICs through integrins becomes passively remodeled or re-organized. Nonetheless, the organization of α-SMA as well as F-actin cables can induce tissue remodeling, potentially through the process described above. Previous TEM studies have shown that the neonatal valve and mature adult valve do indeed have longitudinal arrays of cell-ECM along the tension points of the valve ranging from annulus fibrosae to chordae tendineae (de Vlaming et al., 2012). Thus, blocking VIC shape changes, integrin-mediated cell-ECM interactions, and/or cell-cell adhesions would likely disrupt cell-ECM alignment and result in a phenotypically enlarged, or uncompacted tissue during development. In addition to our current data, recent findings from various *in vivo* mouse models, including perturbations of other genes that cause MVP (such as *FLNA* and *DCHS1*) and *in vitro* 3D models that incorporate tension (Kapacee et al., 2008; Canty et al., 2006; Kadler, 2004; Canty and Kadler, 2002; Kadler et al., 1996), support this hypothesis.

5. Conclusions

The concept that MVP, which is usually diagnosed in aged adults can be rooted in developmental defects may seem paradoxical. However, based on this report, in addition to papers by us and others, we now recognize that MVP has at least two major disease phases that represent cause and effect: 1) *disease inception* that occurs during development and (Durst et al., 2015; Toomer et al., 2019b; Lincoln and Yutzey, 2011; Sauls et al., 2012; Duval et al., 2015) and 2) *disease pathogenesis* that occurs over the lifespan of the affected individual (Sauls et al., 2015; Hulin et al., 2018). *This is akin to a house being built with a faulty structure that will take time to fail.* As such, myxomatous valve disease and MVP must then, by definition, be congenital in nature and influenced by secondary defects (e.g. inflammation, etc.) in valve homeostasis after birth. We posit that valves in MVP patients are not biomechanically inferior because they "degenerate" (as is current dogma), as this would imply destruction of a properly built structure. Rather, valves in MVP patients are built improperly during development and hence "generate" a myxomatous phenotype over time. This distinction is crucial as it places a critical need in understanding how valves are constructed during development with the goal of being able to rectify or correct a tissue that is being built improperly. Herein we have identified a novel mechanism by which Desert Hedgehog signals through the primary cilium in a paracrine, non-cell autonomous manner to activate and stabilize the cytoskeleton (Fig. 7). When perturbed, the actin cytoskeleton is organized improperly resulting in developmental valve defects and *generation* of a myxomatous valve phenotype later in life. As cilia gene defects are common in MVP patients, this study sheds new light on how these structures are functioning in normal valves and the damaging consequences that ciliogenic signaling defects have on actin organization. Finding new methods for organizing and/or stabilizing the actin cytoskeleton may prove beneficial in blunting myxomatous valve progression and functional MVP.

Sources of funding

This work was supported in part by grants from the National Institutes of Health (GM103444 to RAN; P30DK074038 to JL; R01HL131546, P20GM103444, and R01HL127692 to RAN; T32HL007260 to DF and KM; F31HL142159 to DF; RO1HL122906 to AW; T32GM132055 to CG), Veterans Affairs (Merit Award I01 BX000820 to JL), Dialysis Clinic, Inc. (research grant to J.L.), and American Heart Association (19TPA34850095 to RAN, 17CSA33590067 to RAN and JL, and 18PRE34080172 to LG).

Declaration of competing interest

None.

Acknowledgments

Dr. Norris and D. Fulmer designed the research studies and wrote the manuscript. D. Fulmer, Dr. Toomer, J. Glover, Dr. Guo, K. Moore, R. Moore, R. Stairley, C. Gensemer, M.K. Rumph, F. Emetu, C. McDowell, and J. Bian, C. Wang, T. Beck conducted experiments and acquired data. Drs. Norris, Lipschutz, Wessels, Renault and D. Fulmer analyzed and interpreted data and reviewed the manuscript.

Appendix A. Supplementary data

Supplementary data to this article can be found online at https://doi.org/10.1016/j.ydbio.2020.03.003.

References

Aza-Blanc, P., Ci, Kornberg TB., 1999. A complex transducer of the hedgehog signal. Trends Genet. 15 (11), 458–462.
Basso, C., Perazzolo Marra, M., Rizzo, S., De Lazzari, M., Giorgi, B., Cipriani, A., et al., 2015. Arrhythmic mitral valve prolapse and sudden cardiac death. Circulation 132 (7), 556–566.
Bitgood, M.J., Shen, L., McMahon, A.P., 1996. Sertoli cell signaling by Desert hedgehog regulates the male germline. Curr. Biol. : CB 6 (3), 298–304.
Briggs, L.E., Burns, T.A., Lockhart, M.M., Phelps, A.L., Van den Hoff, M.J., Wessels, A., 2016. Wnt/beta-catenin and sonic hedgehog pathways interact in the regulation of the development of the dorsal mesenchymal protrusion. Dev. Dynam. 245 (2), 103–113.
Broekhuis, J.R., Leong, W.Y., Jansen, G., 2013. Regulation of cilium length and intraflagellar transport. Int Rev Cell Mol Biol 303, 101–138.
Burns, T.A., Deepe, R.N., Bullard, J., Phelps, A.L., Toomer, K.A., Hiriart, E., et al., 2019. A novel mouse model for cilia-associated cardiovascular anomalies with a high penetrance of total anomalous pulmonary venous return. Anat. Rec. 302 (1), 136–145.
Butcher, J.T., Markwald, R.R., 2007. Valvulogenesis: the moving target. Philos. Trans. R. Soc. Lond. B Biol. Sci. 362 (1484), 1489–1503.
Butcher, J.T., McQuinn, T.C., Sedmera, D., Turner, D., Markwald, R.R., 2007. Transitions in early embryonic atrioventricular valvular function correspond with changes in cushion biomechanics that are predictable by tissue composition. Circ. Res. 100 (10), 1503–1511.
Butcher, J.T., Norris, R.A., Hoffman, S., Mjaatvedt, C.H., Markwald, R.R., 2007. Periostin promotes atrioventricular mesenchyme matrix invasion and remodeling mediated by integrin signaling through Rho/PI 3-kinase. Dev. Biol. 302 (1), 256–266.
Canty, E.G., Kadler, K.E., 2002. Collagen fibril biosynthesis in tendon: a review and recent insights. Comp. Biochem. Physiol. Mol. Integr. Physiol. 133 (4), 979–985.
Canty, E.G., Starborg, T., Lu, Y., Humphries, S.M., Holmes, D.F., Meadows, R.S., et al., 2006. Actin filaments are required for fibripositor-mediated collagen fibril alignment in tendon. J. Biol. Chem. 281 (50), 38592–38598.
Caradu, C., Couffinhal, T., Chapouly, C., Guimbal, S., Hollier, P.L., Ducasse, E., et al., 2018. Restoring endothelial function by targeting Desert Hedgehog downstream of Klf2 improves critical limb ischemia in adults. Circ. Res. 123 (9), 1053–1065.
Chinchilla, P., Xiao, L., Kazanietz, M.G., Riobo, N.A., 2010. Hedgehog proteins activate pro-angiogenic responses in endothelial cells through non-canonical signaling pathways. Cell Cycle 9 (3), 570–579.
Christensen, S.T., Pedersen, S.F., Satir, P., Veland, I.R., Schneider, L., 2008. The primary cilium coordinates signaling pathways in cell cycle control and migration during development and tissue repair. Curr. Top. Dev. Biol. 85, 261–301.
DAddario, M., Arora, P.D., Fan, J., Ganss, B., Ellen, R.P., McCulloch, C.A., 2001. Cytoprotection against mechanical forces delivered through beta 1 integrins requires induction of filamin A. J. Biol. Chem. 276 (34), 31969–31977.
DAddario, M., Arora, P.D., Ellen, R.P., McCulloch, C.A., 2002. Interaction of p38 and Sp1 in a mechanical force-induced, beta 1 integrin-mediated transcriptional circuit that regulates the actin-binding protein filamin-A. J. Biol. Chem. 277 (49), 47541–47550.

DAddario, M., Arora, P.D., Ellen, R.P., McCulloch, C.A., 2003. Regulation of tension-induced mechanotranscriptional signals by the microtubule network in fibroblasts. J. Biol. Chem. 278 (52), 53090–53097.
Dai, P., Akimaru, H., Tanaka, Y., Maekawa, T., Nakafuku, M., Ishii, S., 1999. Sonic Hedgehog-induced activation of the Gli1 promoter is mediated by GLI3. J. Biol. Chem. 274 (12), 8143–8152.
Davis, E.E., Katsanis, N., 2012. The ciliopathies: a transitional model into systems biology of human genetic disease. Curr. Opin. Genet. Dev. 22 (3), 290–303.
de Vlaming, A., Sauls, K., Hajdu, Z., Visconti, R.P., Mehesz, A.N., Levine, R.A., et al., 2012. Atrioventricular valve development: new perspectives on an old theme. Differentiation 84 (1), 103–116.
Delling, M., DeCaen, P.G., Doerner, J.F., Febvay, S., Clapham, D.E., 2013. Primary cilia are specialized calcium signalling organelles. Nature 504 (7479), 311–314.
Delling, F.N., Gona, P., Larson, M.G., Lehman, B., Manning, W.J., Levine, R.A., et al., 2014. Mild expression of mitral valve prolapse in the Framingham offspring: expanding the phenotypic spectrum. J. Am. Soc. Echocardiogr. 27 (1), 17–23.
Delling, F.N., Rong, J., Larson, M.G., Lehman, B., Fuller, D., Osypiuk, E., et al., 2016. Evolution of mitral valve prolapse: insights from the framingham heart study. Circulation 133 (17), 1688–1695.
Devereux, R.B., Kramer-Fox, R., Kligfield, P., 1989. Mitral valve prolapse: causes, clinical manifestations, and management. Ann. Intern. Med. 111 (4), 305–317.
Dina, C., Bouatia-Naji, N., Tucker, N., Delling, F.N., Toomer, K., Durst, R., et al., 2015. Genetic association analyses highlight biological pathways underlying mitral valve prolapse. Nat. Genet. 47 (10), 1206–1211.
Durst, R., Sauls, K., Peal, D.S., deVlaming, A., Toomer, K., Leyne, M., et al., 2015. Mutations in DCHS1 cause mitral valve prolapse. Nature 525 (7567), 109–113.
Duval, D., Lardeux, A., Le Tourneau, T., Norris, R.A., Markwald, R.R., Sauzeau, V., et al., 2014. Valvular dystrophy associated filamin A mutations reveal a new role of its first repeats in small-GTPase regulation. Biochim. Biophys. Acta 1843 (2), 234–244.
Duval, D., Labbe, P., Bureau, L., Le Tourneau, T., Norris, R.A., Markwald, R.R., et al., 2015. MVP-associated filamin A mutations affect FlnA-PTPN12 (PTP-PEST) interactions. J. Cardiovasc. Dev. Dis. 2 (3), 233–247.
Ehrlicher, A.J., Nakamura, F., Hartwig, J.H., Weitz, D.A., Stossel, T.P., 2011. Mechanical strain in actin networks regulates FilGAP and integrin binding to filamin A. Nature 478 (7368), 260–263.
Farsi, J.M., Aubin, J.E., 1984. Microfilament rearrangements during fibroblast-induced contraction of three-dimensional hydrated collagen gels. Cell Motil. 4 (1), 29–40.
Freed, L.A., Levy, D., Levine, R.A., Larson, M.G., Evans, J.C., Fuller, D.L., et al., 1999. Prevalence and clinical outcome of mitral-valve prolapse. N. Engl. J. Med. 341 (1), 1–7.
Freed, L.A., Benjamin, E.J., Levy, D., Larson, M.G., Evans, J.C., Fuller, D.L., et al., 2002. Mitral valve prolapse in the general population: the benign nature of echocardiographic features in the Framingham Heart Study. J. Am. Coll. Cardiol. 40 (7), 1298–1304.
Friedland-Little, J.M., Hoffmann, A.D., Ocbina, P.J., Peterson, M.A., Bosman, J.D., Chen, Y., et al., 2011. A novel murine allele of Intraflagellar Transport Protein 172 causes a syndrome including VACTERL-like features with hydrocephalus. Hum. Mol. Genet. 20 (19), 3725–3737.
Fulmer, D., Toomer, K., Guo, L., Moore, K., Glover, J., Moore, R., et al., 2019. Defects in the exocyst-cilia machinery cause bicuspid aortic valve disease and aortic stenosis. Circulation 140 (16), 1331–1341.
Gerdes, J.M., Katsanis, N., 2008. Ciliary function and Wnt signal modulation. Curr. Top. Dev. Biol. 85, 175–195.
Gerhardt, C., Leu, T., Lier, J.M., Ruther, U., 2016. The cilia-regulated proteasome and its role in the development of ciliopathies and cancer. Cilia 5, 14.
Goddeeris, M.M., Rho, S., Petiet, A., Davenport, C.L., Johnson, G.A., Meyers, E.N., et al., 2008. Intracardiac septation requires hedgehog-dependent cellular contributions from outside the heart. Development 135 (10), 1887–1895.
Goto, H., Inoko, A., Inagaki, M., 2013. Cell cycle progression by the repression of primary cilia formation in proliferating cells. Cell. Mol. Life Sci. 70 (20), 3893–3905.
Gould, R.A., Yalcin, H.C., MacKay, J.L., Sauls, K., Norris, R., Kumar, S., et al., 2016. Cyclic mechanical loading is essential for rac1-mediated elongation and remodeling of the embryonic mitral valve. Curr. Biol. : CB 26 (1), 27–37.
Guerrero, I., Kornberg, T.B., 2014. Hedgehog and its circuitous journey from producing to target cells. Semin. Cell Dev. Biol. 33, 52–62.
Haycraft, C.J., Zhang, Q., Song, B., Jackson, W.S., Detloff, P.J., Serra, R., et al., 2007. Intraflagellar transport is essential for endochondral bone formation. Development 134 (2), 307–316.
Hildebrandt, F., Benzing, T., Katsanis, N., 2011. Ciliopathies. N Engl J Med. 364 (16), 1533–1543.
Hjortnaes, J., Keegan, J., Bruneval, P., Schwartz, E., Schoen, F.J., Carpentier, A., et al., 2016. Comparative histopathological analysis of mitral valves in barlow disease and fibroelastic deficiency. Semin. Thorac. Cardiovasc. Surg. 28 (4), 757–767.
Horne, T.E., VandeKopple, M., Sauls, K., Koenig, S.N., Anstine, L.J., Garg, V., et al., 2015. Dynamic heterogeneity of the heart valve interstitial cell population in mitral valve health and disease. J. Cardiovasc. Dev. Dis. 2 (3), 214–232.
Hsiao, Y.C., Tuz, K., Ferland, R.J., 2012. Trafficking in and to the primary cilium. Cilia 1 (1), 4.
Hulin, A., Anstine, L.J., Kim, A.J., Potter, S.J., DeFalco, T., Lincoln, J., et al., 2018. Macrophage transitions in heart valve development and myxomatous valve disease. Arterioscler. Thromb. Vasc. Biol. 38 (3), 636–644.
Ishikawa, H., Marshall, W.F., 2011. Ciliogenesis: building the cell's antenna. Nat. Rev. Mol. Cell Biol. 12 (4), 222–234.
Jin, S.C., Homsy, J., Zaidi, S., Lu, Q., Morton, S., DePalma, S.R., et al., 2017. Contribution of rare inherited and de novo variants in 2,871 congenital heart disease probands. Nat. Genet. 49 (11), 1593–1601.
Kadler, K., 2004. Matrix loading: assembly of extracellular matrix collagen fibrils during embryogenesis. Birth Defects Res C Embryo Today 72 (1), 1–11.
Kadler, K.E., Holmes, D.F., Trotter, J.A., Chapman, J.A., 1996. Collagen fibril formation. Biochem. J. 316 (Pt 1), 1–11.
Kapacee, Z., Richardson, S.H., Lu, Y., Starborg, T., Holmes, D.F., Baar, K., et al., 2008. Tension is required for fibripositor formation. Matrix Biol. 27 (4), 371–375.
Karp, N., Grosse-Wortmann, L., Bowdin, S., 2012. Severe aortic stenosis, bicuspid aortic valve and atrial septal defect in a child with Joubert Syndrome and Related Disorders (JSRD) - a case report and review of congenital heart defects reported in the human ciliopathies. Eur. J. Med. Genet. 55 (11), 605–610.
Kim, H.R., Richardson, J., van Eeden, F., Ingham, P.W., 2010. Gli2a protein localization reveals a role for Iguana/DZIP1 in primary ciliogenesis and a dependence of Hedgehog signal transduction on primary cilia in the zebrafish. BMC Biol. 8, 65.
Levine, R.A., Handschumacher, M.D., Sanfilippo, A.J., Hagege, A.A., Harrigan, P., Marshall, J.E., et al., 1989. Three-dimensional echocardiographic reconstruction of the mitral valve, with implications for the diagnosis of mitral valve prolapse. Circulation 80 (3), 589–598.
Levine, R.A., Jerosch-Herold, M., Hajjar, R.J., 2018. Mitral valve prolapse: a disease of valve and ventricle. J. Am. Coll. Cardiol. 72 (8), 835–837.
Li, Y., Klena, N.T., Gabriel, G.C., Liu, X., Kim, A.J., Lemke, K., et al., 2015. Global genetic analysis in mice unveils central role for cilia in congenital heart disease. Nature 521 (7553), 520–524.
Lienkamp, S., Ganner, A., Inversin, Walz G., 2012. Wnt signaling and primary cilia. Differentiation 83 (2), S49–S55.
Lim, S.M., Trzeciakowski, J.P., Sreenivasappa, H., Dangott, L.J., Trache, A., 2012. RhoA-induced cytoskeletal tension controls adaptive cellular remodeling to mechanical signaling. Integr Biol (Camb). 4 (6), 615–627.
Lincoln, J., Yutzey, K.E., 2011. Molecular and developmental mechanisms of congenital heart valve disease. Birth Defects Res A Clin Mol Teratol 91 (6), 526–534.
Liu, A., Wang, B., Niswander, L.A., 2005. Mouse intraflagellar transport proteins regulate both the activator and repressor functions of Gli transcription factors. Development 132 (13), 3103–3111.
Lum, L., Beachy, P.A., 2004. The Hedgehog response network: sensors, switches, and routers. Science 304 (5678), 1755–1759.
Lum, L., Zhang, C., Oh, S., Mann, R.K., von Kessler, D.P., Taipale, J., et al., 2003. Hedgehog signal transduction via Smoothened association with a cytoplasmic complex scaffolded by the atypical kinesin, Costal-2. Mol. Cell. 12 (5), 1261–1274.
Nauli, S.M., Jin, X., AbouAlaiwi, W.A., El-Jouni, W., Su, X., Zhou, J., 2013. Non-motile primary cilia as fluid shear stress mechanosensors. Methods Enzymol. 525, 1–20.
Norris, R.A., Kern, C.B., Wessels, A., Moralez, E.I., Markwald, R.R., Mjaatvedt, C.H., 2004. Identification and detection of the periostin gene in cardiac development. Anat Rec A Discov Mol Cell Evol Biol 281 (2), 1227–1233.
Peng, Y., Song, L., Li, D., Kesterson, R., Wang, J., Wang, L., et al., 2016. Sema6D acts downstream of bone morphogenetic protein signalling to promote atrioventricular cushion development in mice. Cardiovasc. Res. 112 (2), 532–542.
Perloff, J.K., Child, J.S., 1987. Clinical and epidemiologic issues in mitral valve prolapse: overview and perspective. Am. Heart J. 113 (5), 1324–1332.
Rabkin, E., Aikawa, M., Stone, J.R., Fukumoto, Y., Libby, P., Schoen, F.J., 2001. Activated interstitial myofibroblasts express catabolic enzymes and mediate matrix remodeling in myxomatous heart valves. Circulation 104 (21), 2525–2532.
Rabkin-Aikawa, E., Farber, M., Aikawa, M., Schoen, F.J., 2004. Dynamic and reversible changes of interstitial cell phenotype during remodeling of cardiac valves. J. Heart Valve Dis. 13 (5), 841–847.
Samsa, L.A., Givens, C., Tzima, E., Stainier, D.Y., Qian, L., Liu, J., 2015. Cardiac contraction activates endocardial Notch signaling to modulate chamber maturation in zebrafish. Development 142 (23), 4080–4091.
Sandbo, N., Dulin, N., 2011. Actin cytoskeleton in myofibroblast differentiation: ultrastructure defining form and driving function. Transl. Res. 158 (4), 181–196.
Sasaki, H., Nishizaki, Y., Hui, C., Nakafuku, M., Kondoh, H., 1999. Regulation of Gli2 and Gli3 activities by an amino-terminal repression domain: implication of Gli2 and Gli3 as primary mediators of Shh signaling. Development 126 (17), 3915–3924.
Sasaki, N., Kurisu, J., Kengaku, M., 2010. Sonic hedgehog signaling regulates actin cytoskeleton via Tiam1-Rac1 cascade during spine formation. Mol. Cell. Neurosci. 45 (4), 335–344.
Sauls, K., de Vlaming, A., Harris, B.S., Williams, K., Wessels, A., Levine, R.A., et al., 2012. Developmental basis for filamin-A-associated myxomatous mitral valve disease. Cardiovasc. Res. 96 (1), 109–119.
Sauls, K., Toomer, K., Williams, K., Johnson, A.J., Markwald, R.R., Hajdu, Z., et al., 2015. Increased infiltration of extra-cardiac cells in myxomatous valve disease. J. Cardiovasc. Dev. Dis. 2 (3), 200–213.
Seeger-Nukpezah, T., Golemis, E.A., 2012. The extracellular matrix and ciliary signaling. Curr. Opin. Cell Biol. 24 (5), 652–661.
Sekimizu, K., Nishioka, N., Sasaki, H., Takeda, H., Karlstrom, R.O., Kawakami, A., 2004. The zebrafish iguana locus encodes Dzip1, a novel zinc-finger protein required for proper regulation of Hedgehog signaling. Development 131 (11), 2521–2532.
Taipale, J., Chen, J.K., Cooper, M.K., Wang, B., Mann, R.K., Milenkovic, L., et al., 2000. Effects of oncogenic mutations in Smoothened and Patched can be reversed by cyclopamine. Nature 406 (6799), 1005–1009.
Tay, S.Y., Yu, X., Wong, K.N., Panse, P., Ng, C.P., Roy, S., 2010. The iguana/DZIP1 protein is a novel component of the ciliogenic pathway essential for axonemal biogenesis. Dev. Dynam. 239 (2), 527–534.
Toomer, K.A., Fulmer, D., Guo, L., Drohan, A., Peterson, N., Swanson, P., et al., 2017. A role for primary cilia in aortic valve development and disease. Dev. Dynam. 246 (8), 625–634.
Toomer, K.A., Yu, M., Fulmer, D., Guo, L., Moore, K.S., Moore, R., et al., 2019. Primary cilia defects causing mitral valve prolapse. Sci. Transl. Med. 11 (493).

Toomer, K., Sauls, K., Fulmer, D., Guo, L., Moore, K., Glover, J., et al., 2019. Filamin-A as a balance between erk/smad activities during cardiac valve development. Anat. Rec. 302 (1), 117–124.
Veland, I.R., Awan, A., Pedersen, L.B., Yoder, B.K., Christensen, S.T., 2009. Primary cilia and signaling pathways in mammalian development, health and disease. Nephron. Physiol. 111 (3), p39–53.
Versaevel, M., Grevesse, T., Gabriele, S., 2012. Spatial coordination between cell and nuclear shape within micropatterned endothelial cells. Nat. Commun. 3, 671.
Vokes, S.A., McMahon, A.P., 2004. Hedgehog signaling: iguana debuts as a nuclear gatekeeper. Curr. Biol. : CB 14 (16), R668–R670.
Wang, B., Fallon, J.F., Beachy, P.A., 2000. Hedgehog-regulated processing of Gli3 produces an anterior/posterior repressor gradient in the developing vertebrate limb. Cell 100 (4), 423–434.
Wang, C., Low, W.C., Liu, A., Wang, B., 2013. Centrosomal protein DZIP1 regulates Hedgehog signaling by promoting cytoplasmic retention of transcription factor GLI3 and affecting ciliogenesis. J. Biol. Chem. 288 (41), 29518–29529.
Wessels, A., van den Hoff, M.J.B., Adamo, M., Lockhart, M., Sauls, K., Briggs, L.E., et al., 2012. Epicardially-derived fibroblasts and their contribution to the parietal leaflets of the atrioventricular valves in the murine heart. Dev. Biol. 366, 111–124.
Willaredt, M.A., Gorgas, K., Gardner, H.A., Tucker, K.L., 2012. Multiple essential roles for primary cilia in heart development. Cilia 1 (1), 23.
Wolff, C., Roy, S., Lewis, K.E., Schauerte, H., Joerg-Rauch, G., Kirn, A., et al., 2004. iguana encodes a novel zinc-finger protein with coiled-coil domains essential for Hedgehog signal transduction in the zebrafish embryo. Genes Dev. 18 (13), 1565–1576.
Wu, B., Wang, Y., Lui, W., Langworthy, M., Tompkins, K.L., Hatzopoulos, A.K., et al., 2011. Nfatc1 coordinates valve endocardial cell lineage development required for heart valve formation. Circ. Res. 109 (2), 183–192.
Yalcin, H.C., Shekhar, A., McQuinn, T.C., Butcher, J.T., 2011. Hemodynamic patterning of the avian atrioventricular valve. Dev. Dynam. 240 (1), 23–35.
Yu, M., Georges, A., Tucker, N.R., Kyryachenko, S., Toomer, K., Schott, J.J., et al., 2019. Genome-wide association study-driven gene-set analyses, genetic, and functional follow-up suggest GLIS1 as a susceptibility gene for mitral valve prolapse. Circ Genom Precis Med 12 (5), e002497.